High Precision Direct ToF Ranging using CMOS SPAD and Ultra-Short Pulsed Laser

Tsai-Hao Hsu*, Chun-Hsien Liu, Tzu-Hsien Sang, and Sheng-Di Lin

Institute of Electronics, National Yang Ming Chiao Tung University, 1001 University Road, Hsinchu 30010, Taiwan.

Corresponding Author: h124129859.s@gmail.com, telephone: +886-3-5712121#54240

Record single-shot precision of <20 μm for direct-ToF ranging in sub-second integration time has been achieved. By varying the excess bias of SPAD, we found that the FWHM of collected histogram plays a deterministic role on the ranging precision. The effect of target reflectivity, laser repetition rate, and integration time on precision has been unified as a single parameter named effective integration time, T_{eff}. A simple relation between T_{eff} and precision has also been proposed and verified.

I. Introduction

Light-detection and ranging (LiDAR) system plays a key role in various application like auto-driving and satellite ranging, where CMOS single-photon avalanche diodes (SPADs) can be one of the best detectors in the receiver end because of its single-photon sensitivity, excellent timing resolution and easy fabrication in CMOS process. Fast measurement with high ranging precision could trigger various applications [1,2]. In this paper, we investigates the precision of SPAD-based time-of-flight (ToF) ranger as the race on high-precision distance measurement has been ongoing for decades. In terms of cost and system complexity, direct ToF (d-ToF) is highly competitive among various ranging setups and the milli-meter level precision at 50 m distance have been achieved [4-8]. In this work, we demonstrate a record precision of 15.6 μm in half second integration time (T_{int}) with a d-ToF ranger using a CMOS SPAD chip, a 70-ps short-pulse 905-nm laser, and a 10-ps time-bin resolution time-to-digital converter in a TCSPC card.

II. Experiment setup and result

A single SPAD in a 64x128 array chip fabricated with 180-nm BCD process without any customization was used for this ranging experiment [3]. Figure 1 show the chip layout. The chip size including 64x129 SPADs and their quenching, reset, and readout circuits, is about 4.1x5.0 mm^2. The column and row selectors allow us to activate any single SPAD. The respective active size and breakdown voltage are 14 μm and ~ 49.5 V. The dark-count rate, photo-detection probability (PDP) at 905 nm, and deadtime at 6-V excess bias (Vex) are 1 kHz, 9%, and 10 ns, respectively. Thanks to the high sensitivity of SPAD and to avoid pile-up effect in timing histogram, the focal lens in front of the receiver was removed. Figure 2 illustrated our ranging setup including the TCSPC with time-tag time-resolved (TTTR) function to record every count in a long T_{int} (T_L, 100 or 200 seconds here) for subsequent analysis. Figure 3a shows the normalized T_L histograms using 90% target reflectivity (Rt) and 1-MHz laser at the excess bias of 1.7 – 6 V, which resulted the histogram full-width half maximum (FWHM) in the range of ~1300 – 160 ps on the right axis in Figure 3b, together with the bias-dependent PDP and return probability on the left y-axis, denoted as RP, which is defined as the average return counts per fired laser pulse. The PDP in the bias range is about 2%-5%. The RP in the range of

8% - 17% indicates a negligible pile-up effect in the timing histogram, which is particularly important to study the effect of histogram FWHM on the ranging precision.
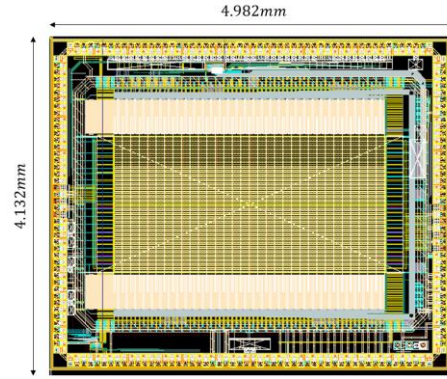

Fig. 1 Layout of the 64X128 SPAD chip.
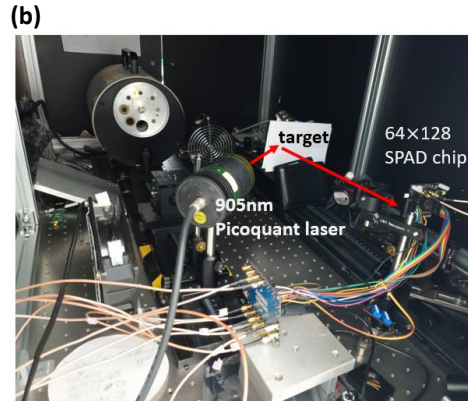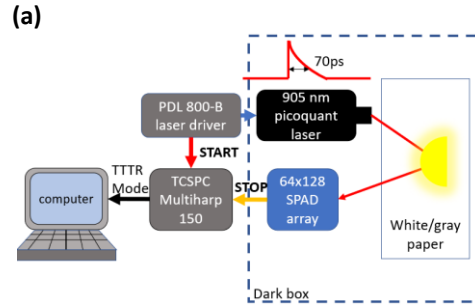
(a)

(b)

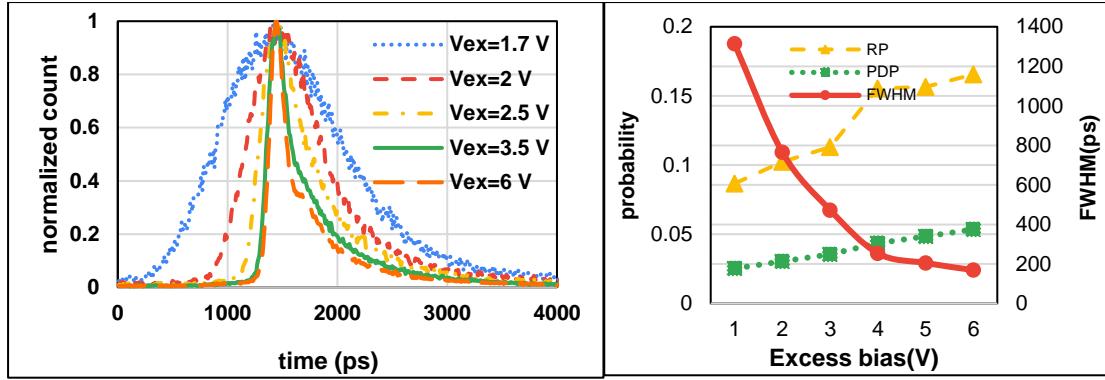**Fig. 2 (a) Block diagram of experiment setup, (b) ranging setup photo.**

Fig. 3 (a) the normalized histogram for 1 second integration time in various Vex, (b) the RP 、 PDP and FWHM of histogram in different excess bias.

Using center-of-mass (CM) method for peak detection, we have obtained the measured distance with the TTTR data for all integration times. Figure 4 shows the standard deviations from >100 measurements, defined as the ranging precision (σ_{CM}), as a function of Tint. The precision σ_{CM} improved dramatically with the increasing Tint. Clearly, the best precision of 15.6 μm was achieved successfully with 6 V Vex, 10 MHz laser, Rt = 90%, and Tint = 0.4 s. The inset on Figure 4 demonstrates that, as expected, the probability density functions of the measured distances follow respective Gaussian distributions very well and the increasing Tint gave the smaller σ_{CM}.
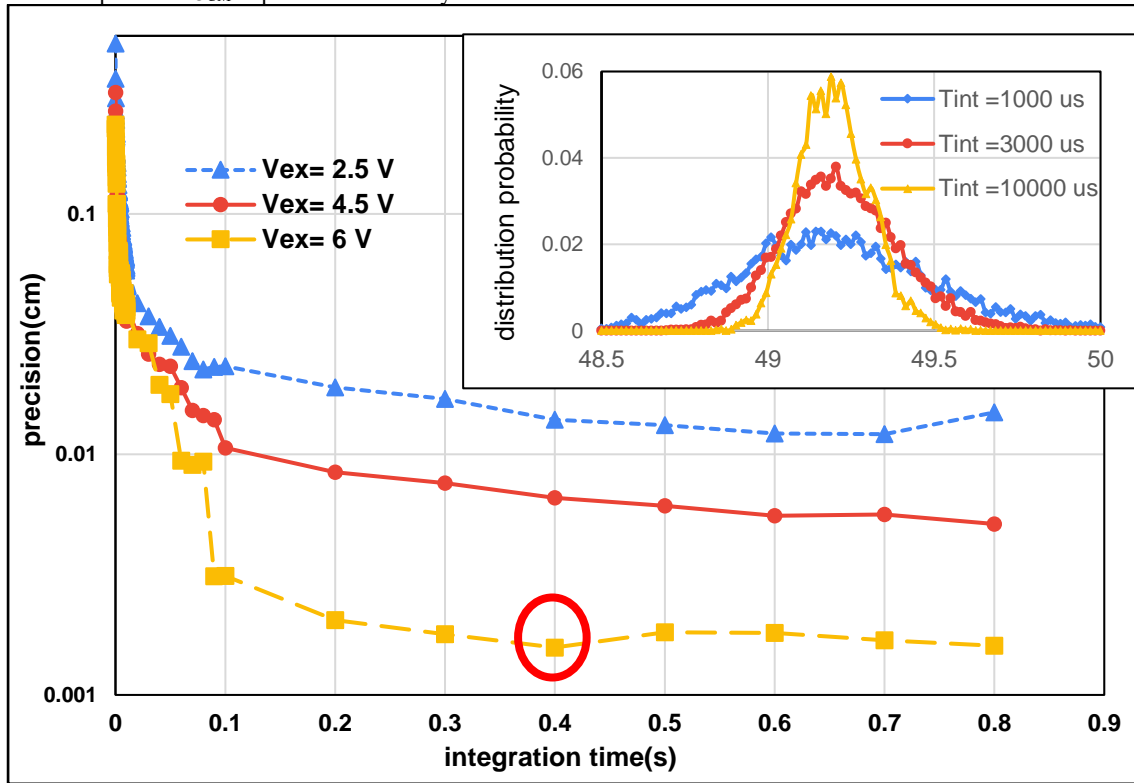

Fig. 4 Precision vs. integration time at various Vex. Inset: measurement distribution at different integration times.

III.   Theoretical model for ranging result

Figure 5a plots the precisions σ_{CM} as a function of FWHM of T_L histograms obtained with three T_{int}. It can be seen that, irrespective of varied T_{int}, σ_{CM} decreases with the decreasing FWHM. To clarify the key factors affecting ranging precision, we introduce the effective integration time, denoted as T_{eff}, defined as,

$$T_{eff} = T_{int} \times RP \times f_L, \quad (1)$$

where f_L is the repetition rate of laser. In fact, T_{eff} is the valid laser counts triggered by the returned photons from target scattering so its physical unit is counts. In this way, we can exclude the effect of the target reflectivity, the SPAD PDP, and the laser repetition rate. Fig. 5b shows a plot similar to that in Fig. 5a but at three T_{eff} instead. The obtained trend is very similar, too, indicating that the FHWM of timing histogram is the dominate factor in ranging precision.
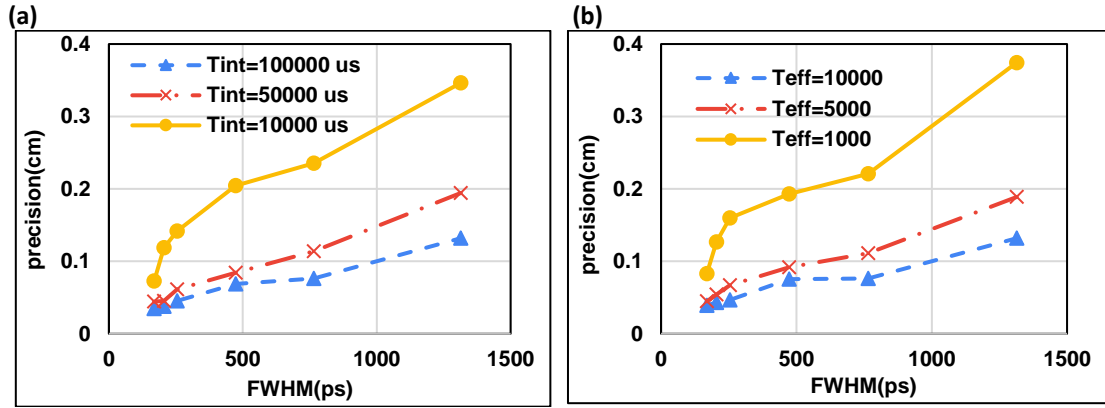
Fig 5. FWHM vs. precision.

Figure 6 clearly exhibits the dominant role of histogram FWHM by plotting the precision at three Vex (or 3 histogram FWHMs) as a function of T_{eff} for a few different ranging conditions, including Rt = 18% or 90% and f_L = 1 or 10 MHz. Obviously, at the same Vex (or the same histogram FWHM), the relation between the measured precision and T_{eff} is the same as all data points fall on the same line. Interestingly, the log-log plot reveals an interesting dependence,

$$\sigma_{CM} \propto T_{eff}^{\frac{-1}{2}}, \qquad (2)$$

After taking the fluctuation of counts in each time bin and calculating the error propagation to our CM method [1], we can approximate the precision σ_{CM} as,

$$\sigma_{CM} \cong \sqrt{\sum_{n=-\frac{N}{2}}^{n=\frac{N}{2}} \left(\frac{n}{c_t}\right)^2 c_n} \propto c_t^{-1/2}, \qquad (3)$$

where explaining the slope = -0.5 in log-log plot in Fig. 6..

Figure 7 summarizes the d-ToF precision as a function of ranging precision [2]. Clearly, our precision is the best among reported works and it could be of high potential for future ranging applications.
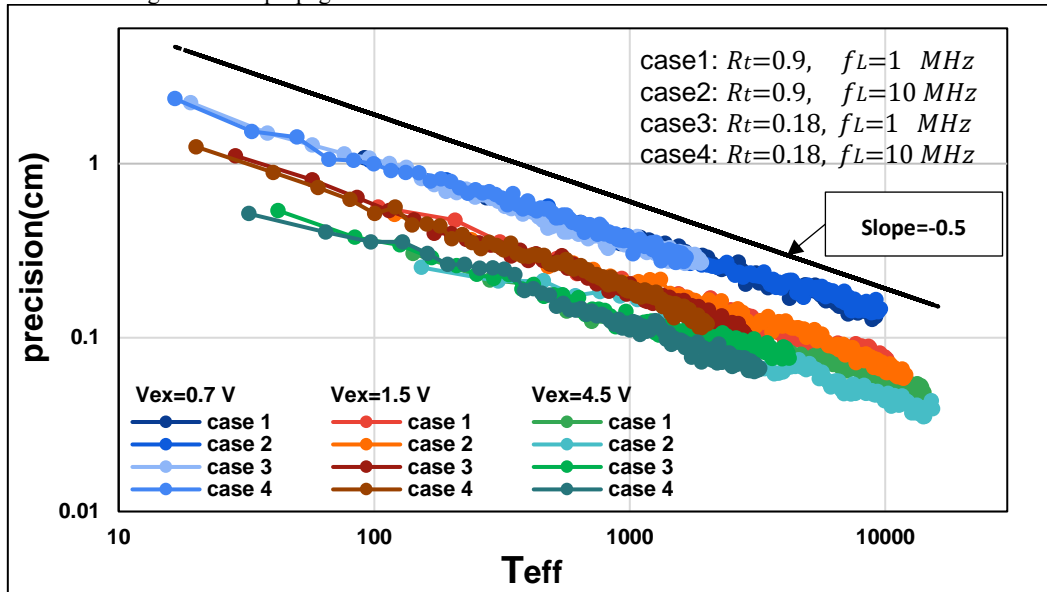

Fig. 6 Precision vs. T_{eff} at three Vex and in four cases in log-log scale
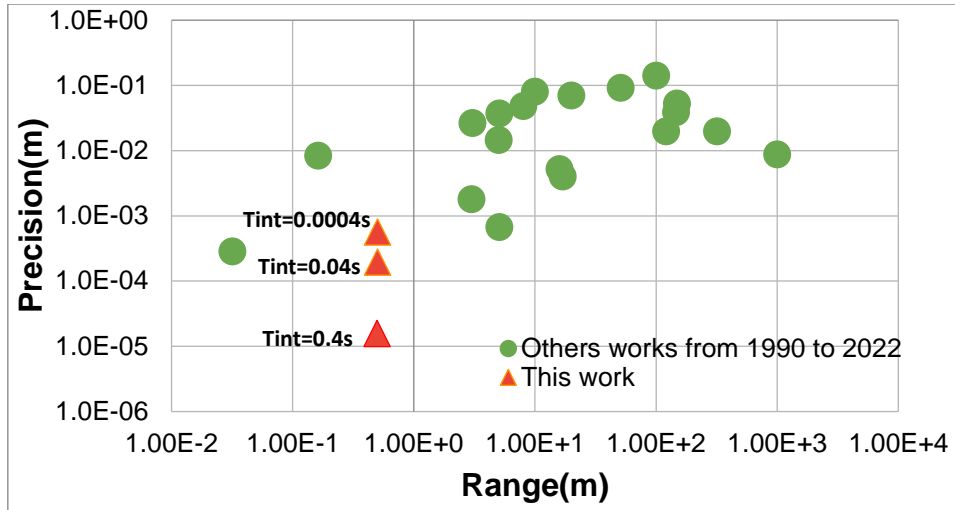
Fig. 7 Precision vs. operating range since 1990 to 2022.

IV. Conclusion

In this work, with 0.4-s Tint、70-ps laser FWHM and 6-V Vex, we have obtained 15.6 μm precision in d-TOF SPAD LiDAR at about 50-cm distance with low background condition. A theoretical model to estimate the relationship between the number of detected photon and precision has been proposed to explain our experimental result.

References

[1] N. Li, C. P. Ho, J. Xue , L. W. Lim, G. Chen, Y. H. Fu, and L. Y. T. Lee "A Progress Review on Solid-State LiDAR and Nanophotonics-Based LiDAR Sensors." Laser & Photonics Reviews, vol. 16, August 2022.

[2] B. Behroozpour, P. A. M. Sandborn, M. C. Wu, and B. E. Boser, "Lidar System Architectures and Circuits," in *IEEE Communications Magazine*, vol. 55, no. 10, pp. 135-142, October. 2017.

[3] P. Chen, C. Liu, A. Hsiao, Y. Tsou, Y. Fang, L. Ko, H. Tsai, C. Tsai, T. Sang, G. Lin, J. Guo, B. Hsiao, and S. Lin, "Minimum ranging time for a LiDAR module using CMOS single-photon avalanche diodes," in Conference on Lasers and Electro-Optics, Technical Digest Series (Optica Publishing Group, 2022), paper JW3A.13, May 2022.

[4] C. Niclass, A. Rochas, P. . -A. Besse and E. Charbon, "Design and characterization of a CMOS 3-D image sensor based on single photon avalanche diodes," in IEEE Journal of Solid-State Circuits, vol. 40, no. 9, pp. 1847-1854, Sept. 2005

[5] S. Kawahito et al., "A CMOS Time-of-Flight Range Image Sensor with Gates-on-Field-Oxide Structure," IEEE Sensors J., vol. 7, no. 12, pp. 1578–86, Dec. 2007.

[6] Z. Chao, S. Lindner, I. M. Antolovic, M. Wolf, and E. Charbon, "A CMOS SPAD Imager with Collision Detection and 128 Dynamically Reallocating TDCs for Single-Photon Counting and 3D Time-of-Flight Imaging," Sensors, vol. 18, Nov. 2018.

[7] C. Zhang, S. Lindner, I. M. Antolović, J. Mata Pavia, M. Wolf and E. Charbon, "A 30-frames/s, 252×144 SPAD Flash LiDAR With 1728 Dual-Clock 48.8-ps TDCs, and Pixel-Wise Integrated Histogramming," in IEEE Journal of Solid-State Circuits, vol. 54, no. 4, pp. 1137-1151, April 2019.

[8] T. Paweł, D. Z. Wziątek, S. Dalyot, T. Boski, and F. P. L.Filho, "A High-Precision LiDAR-Based Method for Surveying and Classifying Coastal Notches," ISPRS International Journal of Geo-Information, vol. 7, no. 8, pp. 295, July 2018.